Water diffusion in a synthetic hectorite by neutron scattering—beyond the isotropic translational model

2008 J. Phys.: Condens. Matter 20 104205

(http://iopscience.iop.org/0953-8984/20/10/104205)

J. Phys.: Condens. Matter **20** (2008) 104205 (10pp) doi:10.1088/0953-8984/20/10/104205

Water diffusion in a synthetic hectorite by neutron scattering—beyond the isotropic translational model

V Marry[1], N Malikova[1,2], A Cadène[1], E Dubois[1], S Durand-Vidal[1], P Turq[1], J Breu[3], S Longeville[2] and J-M Zanotti[2]

[1] Université Pierre et Marie Curie-Paris 6, UMR-UPMC-CNRS-ESPCI 7612, Laboratoire LI2C, Case 51, 4 place Jussieu, Paris F-75005, France
[2] Laboratoire Léon Brillouin, UMR CEA-CNRS 12, CEA Saclay, 91191 Gif-sur-Yvette, France
[3] Institut für Anorganische Chemie der Universität Regensburg, D-93040 Regensburg, Germany

E-mail: marry@ccr.jussieu.fr

Received 16 July 2007, in final form 2 October 2007
Published 19 February 2008
Online at stacks.iop.org/JPhysCM/20/104205

Abstract

A quasi-elastic neutron scattering study of water dynamics confined in a model clay system (a synthetic hectorite with Na^+ compensating counterions) is presented. The neutron spin echo (NSE) data obtained at ambient temperature for the monohydrated and bihydrated hectorite powder are analysed with the help of models taking into account the anisotropy of the system. A powder-averaged two-dimensional (2D) diffusion model applied to the monohydrated state yields a 2D diffusion coefficient in the plane of the clay layers ($D_\parallel$) of 2.8×10^{-10} m^2 s^{-1}, where an isotropic analysis of the data would have underestimated the diffusion coefficient by approximately 25%. In the case of the bihydrated state, the analysis by a model including a possible diffusion perpendicular to the clay layers ($D_\perp$) leads to a range of values for $D_\parallel$ between 3.5 and 8.7×10^{-10} m^2 s^{-1}, depending on the ratio $D_\parallel/D_\perp$. We conclude that simple isotropic analysis can only give a rough estimate (order of magnitude) of the water dynamics in the medium.

(Some figures in this article are in colour only in the electronic version)

1. Introduction

The study of water under nanometric confinement is a long-standing research topic of interest in the fields of catalysis (organic/inorganic), nanofluidics, geology etc. Neutron scattering is perhaps the primary experimental technique for unravelling the mechanistic details of water motion under confinement. This is due to its sensitivity to the self-diffusion of hydrogen atoms and ready access to the appropriate length scale (down to the order of Å). However, as with many other modern experimental techniques, the data interpretation is based on an initial proposal of a possible model, in this case a model of motion. Often more than one model is consistent with the data and other independent pieces of information have to be brought together to narrow down the possibilities. In recent decades, one such additional method has been that of numerical simulation and its importance is ever increasing. In this paper we take the example of a synthetic clay as a water confining matrix. With the aid of structural information on the system and results from microscopic simulation, we assess the most geometrically appropriate translational diffusion model by analysing data from the neutron spin echo technique.

Clay minerals are highly abundant natural materials of interest in several industrial processes. They have applications including catalysis, storage of radioactive waste etc [1–4]. Clays are composed of micrometric particles formed by stacks of negatively charged alumino-silicate layers compensated by cations such as Na^+ and Ca^{2+} [2, 3]. Under conditions of increased relative humidity, these cations become hydrated and the clay thus becomes a matrix containing water confined in parallel planes (ordered in the direction of the clay stacks), with each water plane only a couple of Å in thickness and accommodating only a single or double layer of water molecules. We refer to these states as monohydrated and

bihydrated clay respectively. In this study we use a synthetic hectorite clay [5], which we consider to be a model clay system with a very well defined structure and charge distribution on the clay layers, leading to a highly regular swelling [6], in contrast to its natural counterparts [7, 8].

The literature reports experimental microscopic measurements of water dynamics (on the scale of ps–ns and Å) in several natural clay systems using primarily the time-of-flight technique [9–14] and more recently the neutron spin echo technique [15–17]. In addition, studies of direct comparison of neutron scattering and molecular dynamics simulations are reported [18–21]. For non-oriented or only partially oriented clay samples (powder or pellets), water diffusion coefficients are grossly estimated using the simple isotropic translational diffusion model [10, 11, 14, 19]. In monohydrated clays these are seen to be an order of magnitude lower than in bulk water and in the bihydrated system they are of the order of bulk water, i.e. 10^{-10} m^2 s^{-1} and 10^{-9} m^2 s^{-1} respectively. Studies that attempt to take into account a partial orientation of the clay platelets fail to see a marked difference between the quality of the fits using the more appropriate powder-averaged two-dimensional (2D) translational diffusion and the isotropic diffusion, e.g. [9]. This is also true for neighbouring systems, such as water on the surface of zirconium oxide [22]. On the other hand, studies with macroscopically oriented clay samples attempt to look directly at the anisotropy of water motion in the system [13, 15–17, 21]. However, this necessitates a proper decomposition of the signal scattered in the direction parallel and perpendicular to the clay layers at each scattering angle, which does not seem a trivial task to the authors.

In this study, we go further in the analysis of neutron spin echo signals from a *non-oriented* powder clay sample. As shall be explained, despite the fact that the current data can be analysed using standard isotropic analysis (modelling with a stretched exponential), the resulting diffusion coefficients (isotropic) are *not* consistent with the diffusion coefficients from the geometrically appropriate powder-averaged 2D diffusion model. Throughout our analysis we neglect the rotational motion of water, which on the grounds of intensity is a valid approximation in the low Q region (<1.0 Å^{-1}) [23]. This minimizes the number of adjustable parameters in the model of water motion to one or two parameters for the hectorite monolayer and bilayer respectively.

2. Experimental techniques

2.1. Sample preparation

The clay used in the present study is a synthetic hectorite with a half unit cell composed of $[Na_x]^{inter}[Mg_{3-x}Li_x]^{oct}[Si_4]^{tet}O_{10}F_2$. The negative charge on clay layers is then $0.4e$ per half unit cell. It is compensated by Na^+ cations in the interlayer. The usual structural OH groups in natural clays are replaced by F atoms. Details on the synthesis of fluorohectorites are given elsewhere [5]. Figure 1 shows the atomic detail of two bihydrated clay layers of 16 unit cells each. For a representation of a typical hydrated clay particle (1–2 μm lateral dimensions), this structure must be repeated horizontally several times.

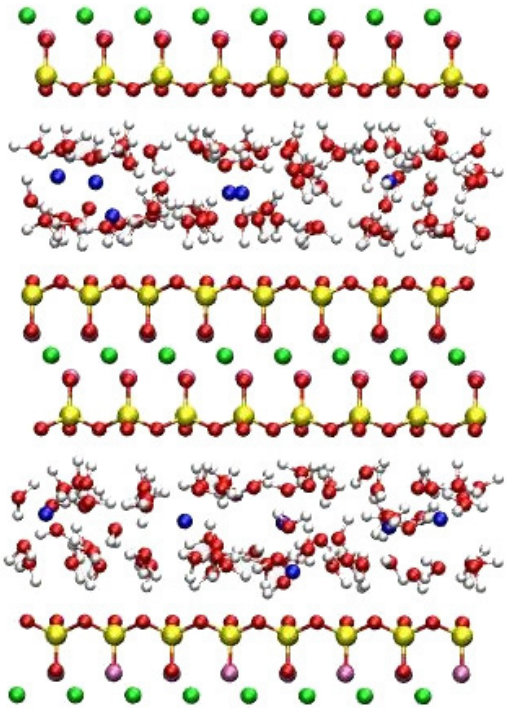

Figure 1. Enlargement of a clay particle: two clay layers of 16 unit cells each are represented in the bihydrated state (snapshot obtained by molecular simulations). Colour code: Mg = green, Si = yellow, O = red, F = mauve, H = white, Na^+ = blue (colour online).

This synthetic clay was chosen because of its remarkable hydration behaviour. The vast majority of the interlayer spaces contains a monolayer of water at HR = 43% and a bilayer at HR = 85%, as shown by neutron and x-ray diffraction measurements [6].

Monolayer and bilayer states are prepared by hydrating for one week the dry hectorite powder in an atmosphere where HR is fixed by saturated salt solutions (K_2CO_3 for HR = 43% and KCl for HR = 85%). Adsorption isotherm and sample weighing show that $n(H_2O)/Na^+$ varies between 3.6 and 4.05 for the monolayer, and between 7.1 and 7.4 for the bilayer.

2.2. Neutron spin echo measurements

Neutron spin echo (NSE) measurements [24, 25] were carried out on the single-detector MUSES spectrometer in LLB, Saclay, France. The polarization of the scattered neutron beam was measured under ambient pressure and temperature at Q values between 0.3 and 1.2 Å^{-1}, in zones of no coherent contribution from the clay structure. These measurements give access to the intermediate incoherent scattering function $I_{inc}(Q, t)$ of protons in the hydrated clay, as these are the atoms with the highest incoherent cross-section in the sample. By combination of both the NSE and NRSE (neutron resonance spin echo) technique [26, 27], measurements for correlation times up to approximately 1000 ps were achieved. Sample cells with a flat geometry were loaded with the non-oriented hectorite powder under a given relative humidity. Considering

the low level of clay hydration and the inherent decrease in the measured polarization when an incoherent scattering signal is exploited, a sample thickness of 5 mm and 2 mm was necessary for monohydrated and bihydrated hectorite respectively. Even under these conditions a collection time of 24 h per Q vector was needed. (We note that these sample thicknesses correspond to a transmission of 0.8 and 0.75 respectively, and as a result multiple scattering could become an issue. However, we are confident that any multiple scattering occurring in these samples does not modify significantly the measured NSE signals as multiple scattering is partly suppressed by the spin-flip scattering [28]. Moreover, the observed relaxation times and their Q-dependence is in very good agreement with data from an independent time-of-flight neutron scattering experiment on the hectorite system, in which the sample thickness corresponded to a transmission superior to 0.9 [6].)

3. Modelling $I_{inc}(Q,t)$

3.1. General background

A theoretical expression for the intermediate scattering function is:

$$I_{\mathrm{inc}}(\mathbf{Q},t) = \frac{1}{N}\sum_{j=1}^{N}\langle \mathrm{e}^{\mathrm{i}\mathbf{Q}\cdot\mathbf{R}_j(t)}\mathrm{e}^{-\mathrm{i}\mathbf{Q}\cdot\mathbf{R}_j(0)}\rangle, \tag{1}$$

where $\mathbf{R}_j(t)$ is the position of scatterer (atom) j at time t, $\mathbf{Q}$ is the wavevector and N is the total number of scatterers in the sample. Equation (1) is a self-correlation function of the positions of individual atoms in the sample. On the basis of their different characteristic timescales, vibrational, rotational and translational atomic motions can be considered as decoupled [23]. $I(\mathbf{Q},t)$ can then be expressed as:

$$I_{\mathrm{inc}}(\mathbf{Q},t) = I_{\mathrm{vib}}(\mathbf{Q},t)I_{\mathrm{rot}}(\mathbf{Q},t)I_{\mathrm{trans}}(\mathbf{Q},t), \tag{2}$$

where $I_{\mathrm{vib}}(\mathbf{Q},t)$ represents intramolecular vibrations of water molecules. As the corresponding energy transfers are beyond the cutoff energy allowed by the NSE spectrometer (a few meV), this type of motion cannot be measured with this technique. $I_{\mathrm{rot}}(\mathbf{Q},t)$ represents the rotation of H atoms around centres of mass of water molecules (water CoM). In the case of bulk or even confined water at ambient temperature, the time-dependent term in $I_{\mathrm{rot}}(\mathbf{Q},t)$ can be considered as sufficiently small to be neglected in the low Q-region ($<$1.0 Å^{-1}). Then the effects of rotational and vibrational motion can be combined in a Q-dependent, but time-independent pre-factor to translational relaxation.

In the case of an isotropic continuous diffusion characterized by a single relaxation time for all water molecules sampled, $I_{\mathrm{trans}}(\mathbf{Q},t)$ takes up the expression:

$$I_{\mathrm{inc}}(\mathbf{Q},t) = I_{\mathrm{inc}}(Q,t) = A(Q)\mathrm{e}^{-(t/\tau)}, \tag{3}$$

where τ is related to the self-diffusion coefficient of the scatterers, by

$$\frac{1}{\tau} = DQ^2. \tag{4}$$

Experimentally it is often difficult to fit $I_{\mathrm{trans}}(\mathbf{Q},t)$ by the above mono-exponential decay. This observation is loosely interpreted by the presence of scatterers with a range of relaxation times. The model is generalized to:

$$I(Q,t) = A(Q)\mathrm{e}^{-(t/\tau)^{\beta}} + B, \tag{5}$$

where the first term is a stretched exponential form characterized by two adjustable parameters, the stretch exponent ($0 < \beta \leqslant 1$) and the relaxation time (τ). The constant background term, B, can be non-zero due to atoms immobile on the timescale of the measurements. The stretched exponential function coincides with a simple exponential decay for $\beta = 1$. In the standard (isotropic) analysis, the apparent diffusion coefficient is taken as the slope of $1/\langle\tau\rangle$ as a function of Q^2 in the limit of $Q^2 \to 0$, where $\langle\tau\rangle = \frac{\tau}{\beta}\Gamma(\frac{1}{\beta})$ and Γ is the gamma function. This apparent diffusion coefficient is interpreted as an average over several types of diffusive motion.

3.2. $I(Q,t)_{inc}$ for water confined in a clay

In the present study, within each clay particle (stack of layers) water diffusion is anisotropic because of the layered structure. Diffusion is allowed parallel to the clay layers but in the direction perpendicular to the clay layers it is bound (refer back to figure 1). On the macroscopic scale we consider the clay sample to be a non-oriented powder, i.e. with all stacking directions of equal probability. As mentioned previously, the quasi-elastic signal from non-oriented powder clay samples is often, to a first approximation, analysed using the simple isotropic model, neglecting the powder effect [10, 11, 14, 19]. We will see in the following sections that taking into account the anisotropy of the system leads to appreciably different results and we estimate the error which can be made in the diffusion coefficient using the isotropic analysis.

In the case of monohydrated hectorite, we consider that water molecules cannot move in the direction perpendicular to the clay layers. Then their motion, within an interlayer, can be considered as a true 2D motion and the results of microscopic simulations clearly support this picture [29]. Considering only diffusive motion (in the limit of low Q), the isotropic expression in equation (3) must be substituted by:

$$\langle I_{2d}(Q,t)\rangle_{\theta} = \tfrac{1}{2}\int_0^{\pi} \mathrm{e}^{-D_{\parallel}Q^2[\sin^2(\theta)]t}\sin\theta\,\mathrm{d}\theta, \tag{6}$$

where $D_{\parallel}$ is the diffusion coefficient parallel to the clay layers and θ is the angle between the wavevector $\mathbf{Q}$ and the direction perpendicular to the clay layers [23, 29]. Note that equation (6) cannot be parametrized in the form of an exponential or stretched exponential decay.

In the case of the bihydrated state, water molecules can move from one water layer to another. Even if this motion is bound, it can have an influence on $I_{\mathrm{trans}}(Q,t)$. Considering a motion in three-dimensions bound only in the direction z [23]:

$$I_{z\text{-bounded}}(Q,t) = \mathrm{e}^{-D_{\parallel}(Q_x^2+Q_y^2)t}\int_0^{L} p(z,t)\cos(Q_z z)\,\mathrm{d}z, \tag{7}$$

where L is the distance of confinement and $p(z,t)$ is the probability of finding an H atom at time t at the position z,

given that it was at the origin at $t = 0$. If the density of H atoms in the interlayer is assumed to be uniform (which is not true in reality, considering the distinguishable water layers seen in simulations, e.g. [30]) and the diffusion equation is verified by $p(z, t|z_0, 0)$, then the probability of finding the atom at (z, t) when at z_0 at $t = 0$, is

$$\frac{\partial p(z,t|z_0,0)}{\partial t} = D_\perp \frac{\partial^2 p(z,t|z_0,0)}{\partial z^2}, \tag{8}$$

where $D_\perp$ is the diffusion coefficient perpendicular to the clay layers. With reflecting boundary conditions on the walls, the above equation has an analytical solution which can be written in the form of a series expansion [23, 31]:

$$p(z,t|z_0,0) = \frac{1}{L} + \frac{2}{L}\sum_{n=1}^{\infty} \cos\left(\frac{n\pi z}{L}\right)\cos\left(\frac{n\pi z_0}{L}\right) \mathrm{e}^{\frac{-n^2\pi^2 D_\perp t}{L^2}}. \tag{9}$$

Then, by integration with respect to z_0 [23]:

$$p(z,t) = \frac{L-z}{L^2} + \sum_{n=1}^{\infty}\left[\frac{L-z}{L^2}\cos\left(\frac{n\pi z}{L}\right) - \frac{1}{nL\pi}\sin\left(\frac{n\pi z}{L}\right)\right]\mathrm{e}^{\frac{-n^2\pi^2 D_\perp t}{L^2}} \tag{10}$$

which leads to:

$$\int_0^L p(z,t)\cos(Q_z z)\,\mathrm{d}z = \frac{1-\cos(Q_z L)}{Q_z^2 L^2} + \sum_{n=1}^{\infty}(1-(-1)^n\cos(Q_z L))\frac{2Q_z^2L^2}{(n^2\pi^2 - Q_z^2L^2)^2}\mathrm{e}^{\frac{-n^2\pi^2 D_\perp t}{L^2}}. \tag{11}$$

In order to take into account the powder effect, we must average this result over θ, the angle between the wavevector $\mathbf{Q}$ and the direction perpendicular to the clay layers. With $Q_z = Q\cos\theta$ and $Q_x^2 + Q_y^2 = Q^2(1-\cos^2\theta)$, we arrive at:

$$\langle I_{z\text{-bounded}}(Q,t)\rangle_\theta = \mathrm{e}^{-D_\parallel Q^2 t}\left[\int_{-1}^{1}\mathrm{e}^{D_\parallel Q^2u^2t}\frac{1-\cos(QuL)}{Q^2u^2L^2}\,\mathrm{d}u + \sum_{n=1}^{\infty}2\mathrm{e}^{\frac{-n^2\pi^2D_\perp t}{L^2}}\int_{-1}^{1}\mathrm{e}^{D_\parallel Q^2u^2t}\times\frac{Q^2u^2L^2(1-(-1)^n\cos(QuL))}{(n^2\pi^2 - Q^2u^2L^2)^2}\,\mathrm{d}u\right], \tag{12}$$

where the variable change $u = \cos\theta$ has been done. The two diffusion coefficients $D_\parallel$ and $D_\perp$ are *a priori* different considering the strong anisotropy of the system.

In the following section we use equations (6) and (12) as the models of water diffusion in monohydrated and bihydrated clay respectively and use them in the analysis of NSE data. These two models are the simplest ones that take into account the anisotropy of the diffusion between clay layers. The motion is considered as purely diffusive despite the presence of clay surfaces with specific interactions, the effect of rotation is neglected (data analysed at low Q). However, they require a minimum number of parameters to fit with experiment ($D_\parallel$ in the monohydrated case, $D_\parallel$ and $D_\perp$ in the bihydrated one). This greatly simplifies the analysis. Moreover, we will see in section 5 that, due to finite experimental precision, two parameters are already too many to lead to a quantitative evaluation of dynamics in the bihydrated state, which means that a more complex model with more adjustable parameters would be even less exploitable.

4. Analysis of data for monohydrated hectorite

NSE data for the monohydrated hectorite are given in figure 2 together with the best fit given by the 2D-averaged model proposed in the previous section. $I(Q, t)$ have been measured for seven Q values: 0.3, 0.4, 0.6, 0.7, 0.85, 1.1 and 1.2 Å^{-1}. The best fit between model and experiment was obtained for $D_\parallel = 2.8 \times 10^{-10}$ m^2 s^{-1}, but the fits remain within the error bars for $D_\parallel$ between 2.4 and 3.2 $\times 10^{-10}$ m^2 s^{-1}. In figure 2, it is clear that the fits are very good for low Q values. At high Q, experimental curves depart from values below the model curves. For better agreement, it is necessary to multiply the modelled curves by a factor inferior to 1. In expression (5), it amounts to decreasing the pre-factor $A(Q)$ and is a consequence of the short-time dynamics discussed later on. Moreover, the fits of experimental and modelled data with equation (5) (isotropic analysis) show that the stretch exponent β decreases in both cases but more so in the experiment. In the case of the 2D model, the motion is purely diffusive (translational), and thus the decrease of β is obviously due to the non-isotropic nature of the diffusion. However, the effect of the powder averaging does not explain the descent in β for the experimental data sets, for which it is significantly more marked.

4.1. Short-time dynamics

In this section, we provide an explanation for the short-time decay causing the decreasing departure of experimental data compared to the 2D translation-only model. For this purpose, molecular simulations of water motion in hectorite have been undertaken. For simulation details on clays, see [18, 19, 32]. In the present study, simulations are used only briefly to help the comparison between an analytical model and experimental data. To avoid the powder effect and rotational dynamics, simulated $I(Q, t)$ were calculated parallel to the clay layers ($Q_\perp = 0$) for water CoMs only.

On figure 3, the simulated $I(Q, t)$ show a fast decay below the first experimentally accessible correlation time (0.76 ps). This is more marked as Q increases. Considering the experimental NSE curves, $I_{\text{vib}}(Q, t)$ can be neglected as it corresponds to energy transfers out of the NSE window. In simulation itself, intramolecular vibrations cannot be seen, because the water model used in simulations (SPC/E) for water is rigid. However, another type of short-time dynamics, the librations (motion of H atoms around a linear arrangement O–H–O involved in a hydrogen bond) can be seen by simulations. The librations can be modelled using the 'relaxing cage model' of Chen, where the vibrations of water molecules within a cage formed by the nearest water molecules are modelled by a harmonic potential [33]. It is likely that this type of motion, about ten times slower than intramolecular vibrations,

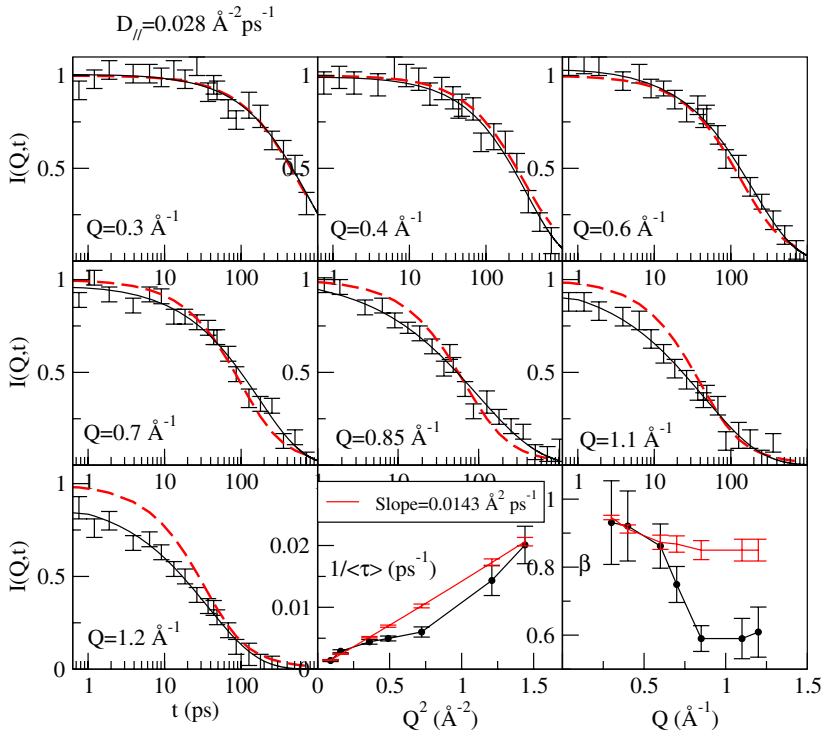

Figure 2. Experimental $I(Q, t)$ curves from NSE for the hectorite monolayer (black data points) with the corresponding isotropic (stretched exponential) fit (plain black line) and curves generated using a powder-averaged 2D model with $D_{\parallel} = 2.8 \times 10^{-10}$ m^2 s^{-1} (dashed red lines). Inverse average relaxation times ($1/\langle\tau\rangle$) and stretch exponent (β) as a function of Q from a fit of the two $I(Q, t)$ series with a single stretched exponential: from experimental data (black circles), from the 2D model (red plus).

can also be seen by experiment. Simulations show that at 0.76 ps, the contribution of librations in $I_{\text{vib}}(Q, t)$ has already reached a plateau. Under the setting used, with the shortest correlation time being close to 1 ps, NSE does not trace the short-time decay, but the measurement is sensitive to it and the experimental curves depart from values below those of the 2D translation-only model.

Short-time dynamics cannot explain the decrease of beta with increasing Q on the fits done between 0.76 and 1013 ps. Eliminating the effect of short-time dynamics only consists in rescaling the experimental curves. It changes neither β, nor τ. Moreover, even if the spectrometer could measure correlation times below 0.76 ps, short-time dynamics would be in any case partially truncated by the experimental cutoff energy, which already prevents us from seeing the more energetic intramolecular vibrations.

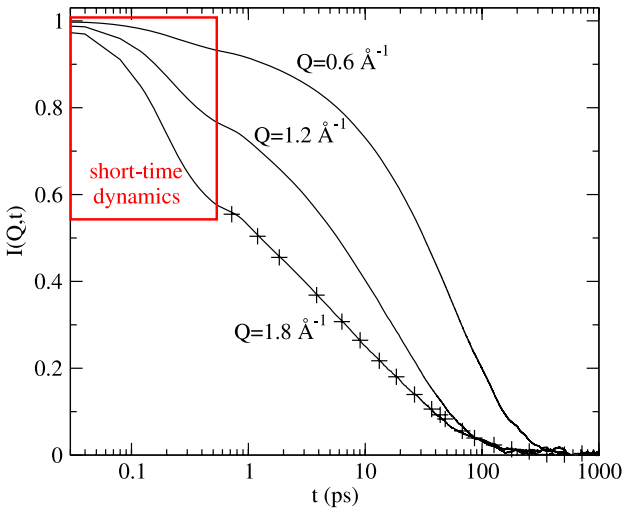

Figure 3. Short-time dynamics. $I(Q, t)$ at $Q = 0.6$, 1.2 and 1.8 Å^{-1} for water mass centres in monohydrated hectorite from microscopic simulation in the direction parallel to clay layers. The zone where short-time dynamics takes place (below 0.5 ps) is indicated in red. Correlation times available from the NSE set-up used are indicated by + on the curve at $Q = 1.8$ Å^{-1}.

4.2. Influence of the experimental cutoff energy

The scattering function $S(Q, \omega)$ is the Fourier transform in time of the intermediate scattering function $I(Q, t)$:

$$S(Q, \omega) = \frac{1}{2\pi} \int_{-\infty}^{+\infty} I(Q, t) \mathrm{e}^{-\mathrm{i}\omega t} \, \mathrm{d}t. \qquad (13)$$

In the NSE experiment however, only the quasi-elastic zone is explored: it means that the measured energy transfers, $\hbar\omega$ (in meV), are confined to a zone we assume to be symmetric around the elastic peak, between $-E_0$ and E_0. The cutoff energy E_0 is a few meV. The NSE spectrometer, then, allows us to measure:

$$I(Q, t) = \frac{P(Q, t)}{P(Q, 0)} = \frac{\int_{-E_0}^{+E_0} S(Q, \omega) \cos(\omega t) \, \mathrm{d}\omega}{\int_{-E_0}^{+E_0} \cos(\omega t) \, \mathrm{d}\omega}, \qquad (14)$$

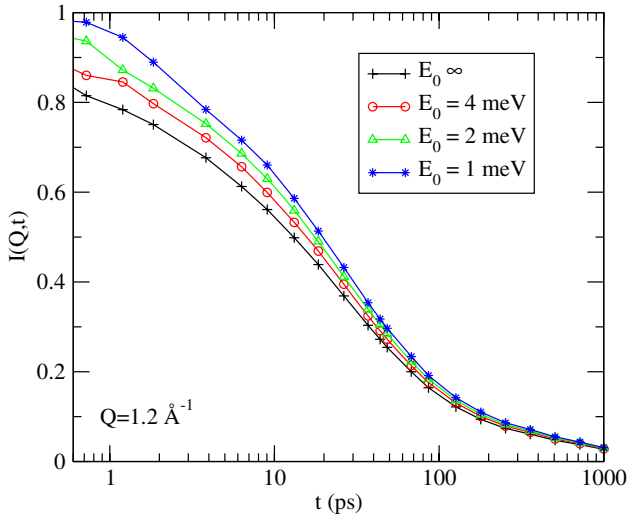

Figure 4. Effect of E_0 on simulated $I(Q,t)$ for $Q = 1.2$ Å^{-1} in the monohydrated hectorite. The curves are represented for the raw simulated $I(Q,t)$ (infinite E_0) and several finite values of E_0 (1, 2 and 4 meV). The correlation times available from the NSE set-up used are indicated by symbols.

where $P(Q,t)$ is the polarization, the measured quantity in NSE. The limited range of measured energy transfers leads to the truncation of very fast dynamics (as intramolecular vibrations, for example). On figure 4, simulated $I(Q,t)$ are represented for $Q = 1.2$ Å^{-1} and various values for E_0: the lower E_0 the higher the departure of the curve. It means that the existence of this cutoff energy will decrease the effect of the librational short-time dynamics on the level of departure of the experimental NSE curves. Fitting the curves of figure 4 by expression (5) shows, however, a negligible influence of E_0 on the obtained β and τ. As in the case of librations, the existence of a cutoff energy can be seen as a simple rescaling of the curves.

4.3. Conclusion on the monohydrated state

In this section on monohydrated hectorite, we have seen that experimental curves are well fitted by the powder-averaged translational model only for small values of Q. When Q increases, experimental $I(Q,t)$ show a faster decrease of the stretch exponent β than in the model and a lower departure level at short times.

Concerning the β behaviour, simulations can help again. Comparison of $I(Q,t)$ from water CoM and from hydrogen atoms shows that rotation slightly decreases β at high Q. Moreover, simulations indicate a non-mono-exponential behaviour even for $I(Q,t)$ calculated from trajectories of water CoMs in the plane parallel to the clay layers. This means that contrary to bulk water, a single relaxation time is not enough to describe the diffusion of water in clays. It is probably the signature of a more complex diffusion mechanism, reflecting the interaction of water with the atomic detail of the clay surfaces [30]. These observations will be studied in detail in our next paper dedicated to simulations; the behaviour of β is put aside for the moment.

In the present study, we have seen that the short-time part of the experimental curves is affected by two phenomena: short-time dynamics and experimental cutoff energy which softens the effects of short-time dynamics. In the end, the combination of these two phenomena makes the *a priori* evaluation of the rescaling, necessary to retrieve the translational model, almost impossible. However, it does not (or only very slightly) affect the values of fitted parameters β and τ. In a first stage, then, we artificially rescaled the experimental curves by multiplying them by the pre-factor $A(Q)$ which allows the best fit with the 2D translational model. The results are given in figure 5. Considering the error bars on the experimental points, the agreement between the model and the rescaled experiment is good.

This means that the model allows the evaluation of a diffusion coefficient in the plane parallel to the clay layers. In the monohydrated state, $D_\parallel = 2.8 \pm 0.4 \times 10^{-10}$ m^2 s^{-1}. At this stage, it is important to note that, because of the powder effect, the diffusion coefficient is no longer given by the slope of $1/\langle\tau\rangle$ as a function of Q^2 in the limit of $Q^2 \to 0$, as it does in a standard isotropic analysis. Indeed, experimental data set aside, a linear fit of $1/\langle\tau\rangle$ resulting from fitting 2D model curves with equation (5) (see figure 2) gives a slope of $D_{3D} = 1.43 \times 10^{-10}$ m^2 s^{-1}, which is not equal to $(D_x + D_y + D_z)/3 = (2D_\parallel + D_\perp)/3 = 2D_\parallel/3 = 1.87 \times 10^{-10}$ m^2 s^{-1} as we could expect. This simple isotropic analysis would lead to an underestimate of the parallel diffusion coefficient by 25%. The powder effect has obviously a non-negligible influence on the modelled $I(Q,t)$. The geometry of the system has then to be properly described in the experimental analysis too if we hope to get quantitative values for $D_\parallel$ better than to an order of magnitude.

5. Analysis of data for bihydrated hectorite

In the case of the bihydrated hectorite, the analysis is complicated by the fact that water molecules can move from one water layer to another, which means that some mobility perpendicular to the clay layers is possible. The system being anisotropic, the motions parallel and perpendicular to the clay surfaces are *a priori* different. By comparing experiment with the model given by equation (12) one should be able to determine the two parameters of interest: $D_\parallel$ and $D_\perp$.

The fit between experiment and model was done for $I(Q,t)$ measured at four Q: 0.55, 0.7, 0.9 and 1.2 Å^{-1}. The value of $L = 6.3$ Å was deduced from the distribution of H atoms in the interlayer space, determined by simulations. This value is close to that calculated by considering that the space accessible to H atoms is the experimental distance between clay layers obtained by x-ray diffraction (15.45 Å) minus the thickness of the clay layer (6.64 Å) minus twice the radius of a surface oxygen atom (2.8 Å), that is to say 6.01 Å. The difference comes from the fact that hydrogen atoms can in fact come closer to the surface especially when situated above the hexagonal cavities formed by the surface O–Si–O.

$D_\parallel$ and $D_\perp$ were allowed to vary from 0 to 2.3×10^{-10} m^2 s^{-1}, the diffusion coefficient of bulk water. Following the same reasoning as in the previous section, we

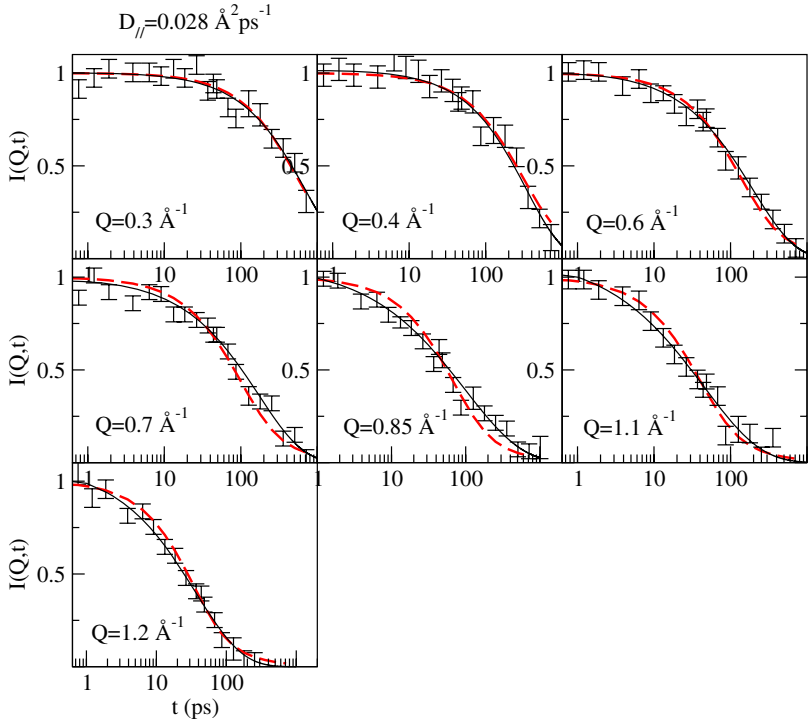

Figure 5. Experimental $I(Q, t)$ curves from NSE for the hectorite monolayer (black data points) and the corresponding isotropic (stretched exponential) fits (plain black line), rescaled in order to fit better the curves generated using the powder-averaged 2D model with $D_{\|} = 2.8 \times 10^{-10}$ m^2 s^{-1} (dashed red lines). Inverse average relaxation times ($1/\langle\tau\rangle$) and stretch exponent (β) as a function of Q are the same as in figure 2.

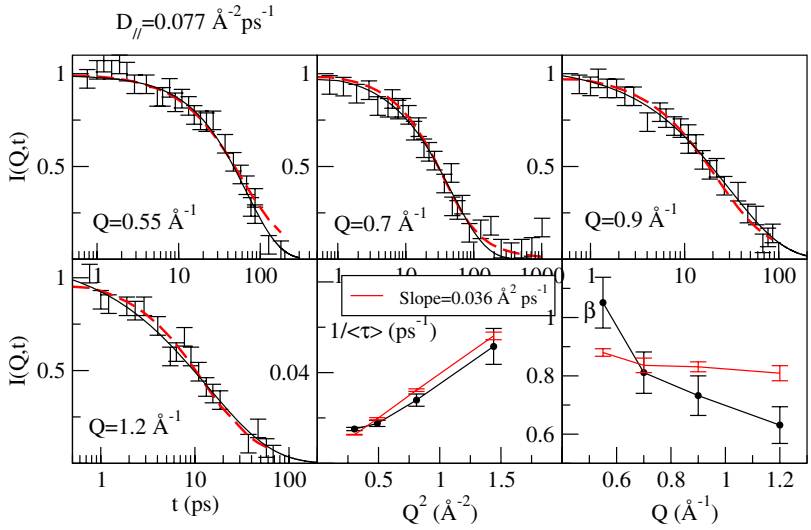

Figure 6. Experimental $I(Q, t)$ curves from NSE for the hectorite bilayer (black data points) with the corresponding isotropic (stretched exponential) fits (plain black line) and curves generated using a powder-averaged bounded model with $D_{\|} = 7.7 \times 10^{-10}$ m^2 s^{-1} and $D_{\perp} = 0$ (dashed red lines). Inverse average relaxation times ($1/\langle\tau\rangle$) and stretch exponent (β) as a function of Q from a fit of the two $I(Q, t)$ series with a single stretched exponential: from experimental data (black circles), from the model (red plus).

allowed the rescaling of experimental curves to fit the 2D model better when necessary, which eliminates the problem of the specific behaviour at short times coupled with the truncation due to E_0.

The best fit was obtained for $D_{\|} = 7.7 \times 10^{-10}$ m^2 s^{-1} and $D_{\perp} = 0$. Fixing $D_{\perp} = 0$, the error on $D_{\|}$ was evaluated as $\pm 1.0 \times 10^{-10}$ m^2 s^{-1} considering the experimental error bars. The curves are given in figure 6. As in the monohydrated system, the diffusion coefficient is not given by the slope of $1/\langle\tau\rangle$ as a function of Q^2 as in the standard (isotropic) analysis. A linear fit of modelled $1/\langle\tau\rangle$ leads to a slope of $D_{3D} = 3.6 \times 10^{-10}$ m^2 s^{-1} which underestimates the expected value for D_{3D}, $(D_x + D_y + D_z)/3 = (2D_{\|} + D_{\perp})/3 = 2D_{\|}/3 = 5.1 \times 10^{-10}$ m^2 s^{-1} by 30%.

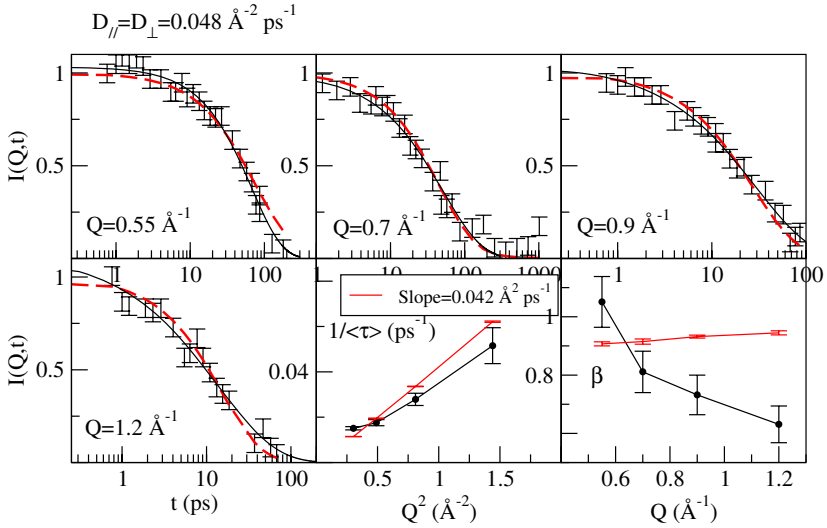

Figure 7. Experimental $I(Q, t)$ curves from NSE for the hectorite bilayer (black data points) with the corresponding isotropic (stretched exponential) fits (plain black line) and curves generated using a powder-averaged bounded model with $D_{\|} = D_{\perp} = 4.8 \times 10^{-10}$ m^2 s^{-1} (dashed red lines). Inverse average relaxation times $(1/\langle\tau\rangle)$ and stretch exponent (β) as a function of Q from a fit of the two $I(Q, t)$ series with a single stretched exponential: from experimental data (black circles), from the model (red plus).

However, the above result is not very realistic. Indeed, simulations show that water molecules diffuse quite easily perpendicularly to the clay layers, even if it is not obvious how to evaluate a perpendicular diffusion coefficient. Considering the experimental error bars and the fact that the results are available only at four Q values, several other acceptable fits are also possible. Fits were carried out for increasing values of $D_{\perp}$, leading to decreasing values of $D_{\|}$. Most of these fits are of sufficient quality. For example, figure 7 shows the comparison between experiment and model for $D_{\perp} = D_{\|}$. In this condition, the best fit was obtained for $D_{\perp} = D_{\|} = 4.8 \times 10^{-10}$ m^2 s^{-1}. Even if this fit is poorer than in figure 6 (in particular, β increases a little instead of decreasing as in the experiment or in the model with $D_{\perp} = 0$) it still works well enough.

When increasing the value of $D_{\perp}$ beyond 4.8×10^{-10} m^2 s^{-1}, $D_{\|}$ obtained by the fit procedure tends finally towards a constant value 3.5×10^{-10} m^2 s^{-1} which is reached for $D_{\perp} > 15 \times 10^{-10}$ m^2 s^{-1}. It would correspond to a perpendicular diffusion coefficient more than four times higher than the parallel one. Here again, simulations are needed to help us know if this situation is realistic or not. In particular, the assumption that the motion perpendicular to the clay layers is continuous is too simplistic. The real motion of hydrogen atoms is probably a combination of continuous and jump diffusion, depending on the preferential interactions with the surfaces, and rotation.

To conclude this section on the bihydrated state, it appears that, despite the low number of parameters in the proposed model, experimental precision is insufficient to allow us to discriminate between the various possible combinations ($D_{\|}$, $D_{\perp}$). Indeed the present study leads finally to a diffusion coefficient parallel to the clay layers, varying between 3.5 and 8.7×10^{-10} m^2 s^{-1}, with a better agreement between model and experiment for the high values of $D_{\|}$.

6. Conclusion

Water dynamics confined in clays was studied by neutron spin echo on a sample of synthetic hectorite with Na^+ compensating counterions. Using a model of powder-averaged 2D diffusion with a single parameter ($D_{\|}$) for the monohydrated clay, the agreement between the data and the model is very good. This is the case after a rescaling of the experimental curves, taking into account short-time relaxations due to librations partly truncated by the cutoff energy of the NSE spectrometer. This model yields a 2D diffusion coefficient in the plane of the clay layers ($D_{\|}$) of 2.8×10^{-10} m^2 s^{-1}. A standard isotropic analysis leads to an underestimation of the relaxation times and the corresponding diffusion coefficients by approximately 25%.

In the case of the bihydrated state, the powder-averaged 2D model contains two parameters, $D_{\|}$ and $D_{\perp}$. We show that diffusion coefficients are sensitive to the ratio $D_{\|}/D_{\perp}$. An isotropic analysis of the experimental data leads to 3.6 $\times 10^{-10}$ m^2 s^{-1} for D_{3D}, without any information on $D_{\|}$ and $D_{\perp}$. Assuming that $D_{\perp} = 0$, isotropic analysis would give $D_{\|} = 3D_{3D}/2 = 5.4 \times 10^{-10}$ m^2 s^{-1}, which is more than 30% lower than the value obtained with the powder-averaged 2D model (7.7×10^{-10} m^2 s^{-1}). In fact, for $D_{\perp} \neq 0$, we can only give a range of values from 3.5 to 8.7×10^{-10} m^2 s^{-1} for $D_{\|}$, depending on the ratio $D_{\|}/D_{\perp}$. The question that remains is how to discriminate between the possible combinations of $D_{\|}$ and $D_{\perp}$.

Further improvement of the model, apart from finding the appropriate ratio of $D_{\|}$ and $D_{\perp}$, consists in lifting the assumption that the diffusion is continuous in the three directions of space (e.g. the possibility of jump diffusion) and incorporating rotation effects for the analysis of high Q data. All this, however, has to be done with a minimal number of adjustable parameters in the model, some parameters being fixed thanks to auxiliary information from

other techniques. For this purpose, we expect an input from molecular simulations, as has been shown previously [6]. We feel that discriminating between the different models solely on the basis of neutron spin echo data is possible only with a significantly better statistics on the individual data points, which is currently not achievable with reasonable data collection times. In a somewhat different direction, we envisage making measurements of the elastic intensity as a function of experimental resolution on a time-of-flight neutron spectrometer. This could highlight directly the difference between powder-averaged 2D and isotropic diffusion, as suggested theoretically by Lechner [34].

Acknowledgment

We acknowledge ANDRA (Agence Nationale pour la Gestion des Déchets Radioactifs) for their support.

References

[1] Fowden L, Barrer R M and Tinker P B (ed) 1984 *Clay Minerals: Their Structure, Behaviour and Use* (London: Royal Society)
[2] Velde B 1992 *Introduction to Clay Minerals* (London: Chapman and Hall)
[3] Giese R F and van Oss C J 2002 Colloid and surface properties of clays and related minerals *Surfactant Science Series* vol 105 (New York: Dekker)
[4] 2001 *ANDRA: Referentiel Materiaux, Tome 2: Les Materiaux argileux* Rapport C.RP.AMAT.01.060
[5] Breu J, Seidl W, Stoll A J, Lange K G and Probst T U 2001 Charge homogeneity in synthetic fluorohectorite *Chem. Mater.* **13** 4213–20
[6] Malikova N, Cadène A, Dubois E, Marry V, Durand-Vidal S, Turq P, Breu J, Longeville S and Zanotti J-M 2007 Water diffusion by quasi-elastic neutron scattering in a synthetic hectorite—a model clay system *J. Phys. Chem.* C **111** 17603
[7] Weaver C E 1956 The distribution and identification of mixed-layer clays in sedimentary rocks *Am. Mineral.* **41** 202–21
[8] Ferrage E, Lanson B, Sakharov B A and Drits V A 2005 Investigation of smectite hydration properties by modeling experimental x-ray diffraction patterns: part I. Montmorillonite hydration properties *Am. Mineral.* **90** 1358–74
[9] Cebula D J, Thomas R K and White J W 1981 Diffusion of water in li-montmorillonite studied by quasielastic neutron scattering *Clays Clay Minerals* **29** 241–8
[10] Tuck J J, Hall P L, Hayes M H B, Ross D K and Poinsignon C 1984 Quasi-elastic neutron-scattering studies of the dynamics of intercalated molecules in charge-deficient layer silicates, part 1. Temperature dependence of the scattering from water in Ca-exchanged montmorillonite *J. Chem. Soc. Faraday Trans.* 1 **80** 309–24
[11] Tuck J J, Hall P L, Hayes M H B, Ross D K and Hayter J B 1985 Quasi-elastic neutron-scattering studies of the dynamics of intercalated molecules in charge-deficient layer silicates, part 2. High-resolution measurements of the diffusion of water in montmorillonite and vermiculite *J. Chem. Soc. Faraday Trans.* 1 **81** 833–46
[12] Poinsignon C, Estrade-Szwarckopf J, Conard J and Dianoux A J 1987 Water dynamics in the clay–water system: a quasielastic neutron scattering study *Proc. Int. Clay Conf. (Denver, 1985)* pp 284–91
[13] Swenson J, Bergman R and Howells W S 2000 Quasielastic neutron scattering of two-dimensional water in a vermiculite clay *J. Chem. Phys.* **113** 2873–9
[14] Chakrabarty D, Gautam S, Mitra S, Gil A, Vicente M A and Mukhopadhyay R 2006 Dynamics of absorbed water in saponite clay: neutron scattering study *Chem. Phys. Lett.* **426** 296–300
[15] Swenson J, Bergman R and Longeville S 2001 A neutron spin-echo study of confined water *J. Chem. Phys.* **115** 11299–305
[16] Mamontov E 2000 Quasielastic neutron scattering of two-dimensional water in a vermiculite clay *J. Chem. Phys.* **113** 2873 (Comment)
Mamontov E 2001 A neutron spin-echo study of confined water *J. Chem. Phys.* **115** 11299 (Comment)
Mamontov E 2004 *J. Chem. Phys.* **121** 9193–4
[17] Swenson J, Bergman R, Howells W S and Longeville S 2000 Quasielastic neutron scattering of two-dimensional water in a vermiculite clay *J. Chem. Phys.* **113** 2873 (Response to Comment)
Swenson J, Bergman R, Howells W S and Longeville S 2001 A neutron spin-echo study of confined water *J. Chem. Phys.* **115** 11299 (Response to Comment)
Swenson J, Bergman R, Howells W S and Longeville S 2004 *J. Chem. Phys.* **121** 9195
[18] Malikova N, Cadène A, Marry V, Dubois E, Turq P, Zanotti J-M and Longeville S 2005 Diffusion of water in clays—microscopic simulation and neutron scattering *Chem. Phys.* **317** 226–35
[19] Malikova N, Cadène A, Marry V, Dubois E and Turq P 2006 Diffusion of water in clays on the microscopic scale: modeling and experiment *J. Phys. Chem.* B **110** 3206–14
[20] Skipper N T, Lock P A, Titiloye J O, Swenson J, Mirza Z A, Howells W S and Fernandez-Alonso F 2006 The structure and dynamics of 2-dimensional fluids in swelling clays *Chem. Geol.* **230** 182–96
[21] Michot L J, Delville A, Humbert B, Plazanet M and Levitz P 2007 Diffusion of water in a synthetic clay with tetrahedral charges by combined neutron time of flight measurements and molecular dynamics simulations *J. Phys. Chem.* C **111** 9818–31
[22] Mamontov E 2004 Dynamics of surface water in ZrO_2 studied by quasi-elastic neutron scattering *J. Chem. Phys.* **121** (18) 9087–97
[23] Bée M 1988 *Quasi-Elastic Neutron scattering; Principles and Applications in Solid State Chemistry, Biology and Material Science* (Bristol: Hilger)
[24] Mezei F 1972 Neutron spin echo: a new concept in polarized thermal neutron techniques *Z. Phys.* **255** 146–60
[25] Mezei F 1980 Neutron spin echo spectroscopy *Lecture Notes in Physics* vol 128 (Berlin: Springer)
[26] Gähler R and Golub R 1987 A high resolution neutron spectroscopy for quasielastic scattering on the basis of spin-echo and magnetic resonance *Z. Phys.* B **65** 269–73
[27] Gähler R and Golub R 1988 Neutron resonance spin-echo, bootstrap method for increasing the effective magnetic-field *J. Physique* **49** 1195–202
[28] Wischnewski A, Monkenbusch M, Willner L, Richter D and Kali G 2003 Direct observation of the transition from free to constrained single-segment motion in entangled polymer melts *Phys. Rev. Lett.* **90** 058302
[29] Malikova N 2005 *Dynamique de l'eau et des ions dans les argiles de type montmorillonite par simulation microscopique et diffusion quasi-élastique des neutrons PhD Thesis* Université Pierre et Marie Curie (Paris 6) available at http://www.li2c.upmc.fr/theses.html (in English)
[30] Marry V and Turq P 2002 Microscopic simulation of structure and dynamics of water and counterions in a monohydrated montmorillonite *J. Chem. Phys.* **117** 3454–63

[31] Tikhonov A N and Samarskii A A 1990 *Equations of Mathematical Physics* (New York: Dover)
[32] Marry V, Turq P, Cartailler T and Levesque D 2002 Microscopic simulation for structure and dynamics of water and counterions in a monohydrated montmorillonite *J. Chem. Phys.* **117** 3454
[33] Chen S-H, Liao C, Sciortino F, Gallo P and Tartaglia P 1999 Model for single-particle dynamics in supercooled water *Phys. Rev.* E **59** 6708–14
[34] Lechner R E 1995 Effects of low-dimensionality in solid-state protonic conductors *Solid State Ion.* **77** 280–6